Enhanced low voltage nonlinearity in resonant tunneling metal-insulator-insulator-metal nanostructures

A.D. Weerakkody[1], N. Sedghi[1], I.Z. Mitrovic[1], H. van Zalinge[1], I. Nemr Noureddine[1], S. Hall[1], J.S. Wrench[2], P.R. Chalker[2], L.J. Phillips[3], R. Treharne[3], K. Durose[3]

[1]*University of Liverpool, Department of Electrical Engineering & Electronics, Liverpool, UK*
[2]*Centre for Materials and Structures, School of Engineering, University of Liverpool, Liverpool, UK*
[3]*Stephenson Institute for Renewable Energy, University of Liverpool, Liverpool, UK*
E-mail address of corresponding author: d.a.d.weerakkody@liverpool.ac.uk

The electrical properties of bi-layer Ta_2O_5/Al_2O_3 and Nb_2O_5/Al_2O_3 metal-insulator-insulator-metal nanostructures as rectifiers have been investigated. The ultra-thin (1-6 nm) insulator layers were deposited by atomic-layer deposition or rf magnetron sputtering with Al as metal contacts. Variable angle spectroscopic ellipsometry was performed to extract the optical properties and band gap of narrow band gap insulator layers while the surface roughness of the metal contacts was measured by atomic force microscopy. Superior low voltage large signal and small signal nonlinearities such as asymmetry of 18 at 0.35 V, rate of change of non-linearity of 7.5 V^{-1}, and responsivity of 9 A/W at 0.2 V were observed from the current-voltage characteristics. A sharp increase in current at ~2 V on Ta_2O_5/Al_2O_3 device can be ascribed to resonant tunneling.

Keywords: metal-insulator-insulator-metal nanorectifiers, nonlinearity, resonant tunneling

1. Introduction

Metal–insulator–metal (MIM) rectifying devices using double [1–5], triple [6] or quadruple [5] insulator layers are currently the focus of attention for the development of next-generation antenna-coupled infrared detectors [7] and optical rectennas [8]. The interest is driven by their distinctive attributes, such as nanoscale footprint, room temperature operation, zero bias voltage requirement, and ease of integration with Complementary Metal Oxide Semiconductor (CMOS) technology. Superior diode characteristics such as large responsivity, asymmetry and nonlinearity can be achieved via thermionic emission and quantum mechanical tunneling, however for less temperature dependent high-speed operation [9], the dominant conduction should be quantum tunneling. Devices with two insulator layers, viz. metal–insulator–in sulator–metal (MIIM) enhance the rectification by increasing the nonlinearity of the current–voltage (*IV*) characteristics. There are two mechanisms that allow MIIM rectifiers to have a high nonlinearity while keeping the resistance low [1–5]: (i) use of resonant tunneling (RT) of electrons through a quantum well formed between the two insulators (Fig. 1a). This occurs when the metal Fermi level on the higher barrier side is biased positive creating a right-triangular well at the interface of the two insulators. When an allowed energy level in the quantum well aligns with the metal Fermi level on the negative side, it causes a sharp turn-on of the rectifier; (ii) use of step tunneling (ST) occurs for the opposite bias polarity (Fig. 1b), when an abrupt increase in current occurs, when the metal Fermi level on the higher barrier side rises above the conduction band of the lower barrier, thereby decreasing the tunnel distance. In a particular device, the choice of insulator materials, metals and thicknesses determines the mechanism that dominates. The highest reported rectification parameters for MIIM devices based on $Cr/Al_2O_3/HfO_2/Cr$ are: asymmetry 10 @ 3 V, and responsivity <2.5 A/W for the range of voltages 0.5–2.5 V [3]. A responsivity of 11 A/W at 0.02 V has been predicted from simulations on 4 nm resonant tunneling $W/Nb_2O_5/Ta_2O_5/W$, however not experimentally demonstrated [4]. Even for bilayer Ta_2O_5/Al_2O_3 MIIMs with dissimilar metal electrodes of work function difference of 0.6 eV, the highest reported low voltage (<0.8 V) asymmetry is 10 [1,2,5].

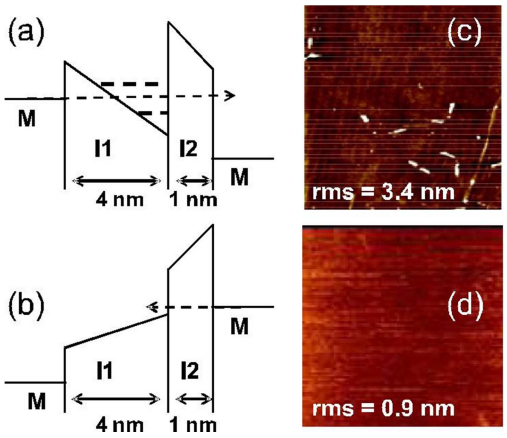

Fig. 1. Energy band diagram of the MIIM structure (a) resonant tunneling in forward bias (b) step tunneling in reverse bias. AFM images of the Al blanket films (c) before, and (d) after optimizing the thermal evaporation parameters. The scanned area is 40 μm × 40 μm.

This paper demonstrates fabrication of bi-layer Ta_2O_5/Al_2O_3 and Nb_2O_5/Al_2O_3 nanostructures using atomic-layer deposition (ALD) and rf sputtering with a focus on achieving low voltage nonlinearity due to the effect of resonant tunneling. We observe superior low voltage asymmetry (18 @ 0.35 V) and responsivity (9 A/W @ 0.2 V) for Ta_2O_5/Al_2O_3 and Nb_2O_5/Al_2O_3 MIIM devices respectively, fabricated using Al metal electrodes.

2. Device fabrication

MIIM devices were fabricated on 4 cm × 4 cm cleaned Corning glass substrates with an rms surface roughness of 0.32 nm. Surface roughness was extracted by both variable angle spectroscopic ellipsometry (VASE) and atomic force microscopy (AFM). Room temperature VASE measurements were performed in the energy range 0.7–5.1 eV and three angles 65°, 70° and 75° to maximize the accuracy in extracting thickness, optical properties and band gap of Nb_2O_5 and Ta_2O_5 layers. The 60 nm thick Al metal contacts were deposited by thermal evaporation and defined either by photolithography or shadow mask. The rms surface roughness after Al evaporation was found to improve substantially from 3.40 nm (Fig. 1c) to 0.87 nm (Fig. 1d) using a lower evaporation rate of 0.4 nm/s. The surface roughness of the substrate and the bottom metal contact was found to have a large impact on device performance in agreement with recent work of Alimardani et al. [10].

We have previously reported theoretical calculations using the multi-barrier transfer matrix method [11], that 1 nm of Al_2O_3 and 3–6 nm of Ta_2O_5 or Nb_2O_5 using Al, can bring optimum low voltage rectification performance. Hence, these thicknesses were used as nominal values for depositing insulators either by ALD or rf magnetron sputtering. The dry etching of Al native oxide was done using Ar plasma at a power of 50 W for 35 min. Room (293 K) and high temperature (293–370 K) current–voltage measurements were performed on fabricated devices in a dark probe station using the Agilent B1500 semiconductor parameter analyzer.

3. Results and discussion

3.1 Optical properties of Ta_2O_5 and Nb_2O_5 films

Optical properties and band gap of Ta_2O_5 and Nb_2O_5 were deter-mined from VASE measurements on bulk oxide films (≥10 nm) deposited by ALD on Si reference samples. The dielectric function of the Si film with the native oxide as Cauchy layer (1.34 nm) was modeled first. Then, another Cauchy layer was added and fit-ted for the thickness of Ta_2O_5 (9.9 nm), or Nb_2O_5 (32.7 nm). Subsequently, the optical constants (real and imaginary parts of the dielectric function) were extracted. The dielectric function converts to refractive index (n) and extinction coefficient (k) using the Kramers–Kronig [12] relations. The absorption coefficient (α) is calculated from the extinction coefficient as a = 4πk/λ, where k is wavelength. The n, k and a vs photon energy (E) plots are shown in Fig. 2a–c respectively. The band gap can be estimated by linear extrapolation of the segments on the curves in the non-absorbing regions, and is found to be 3.71 eV for Nb_2O_5 and 4.45 eV for Ta_2O_5.

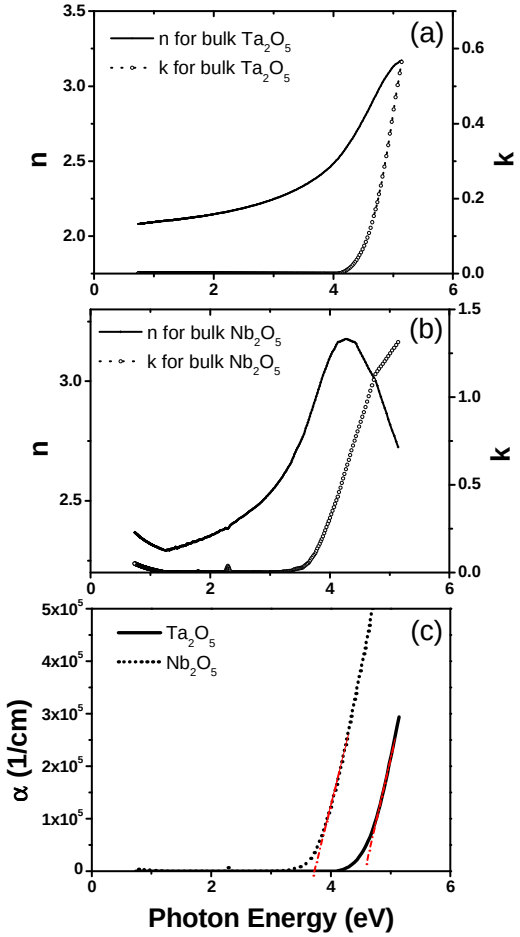

Fig.2: Refractive index (n) and extinction coefficient (k) vs photon energy for bulk (> 10 nm) (a) Ta_2O_5, and (b) Nb_2O_5 films. (c) The extraction of band gap from the absorption coefficient vs photon energy plots for respective Ta_2O_5 and Nb_2O_5 films deposited by ALD.

3.2 Rectification parameters of fabricated Ta_2O_5/Al_2O_3 and Nb_2O_5/Al_2O_3 MIIM devices

The typical current density vs. voltage (*JV*) characteristics of the MIIM devices with 4 nm Ta_2O_5

or Nb_2O_5, 1 nm deposited Al_2O_3 and ~1.6 nm native Al_2O_3 are shown in Fig. 3(a). It can be seen that Nb_2O_5/Al_2O_3 MIIM device shows larger current due to smaller band gap (see Fig. 2(c)) and smaller barrier height at the Al/Nb_2O_5 (up to 0.2 eV) than that at the Al/Ta_2O_5 (~ 0.5 eV) interface [4,13]. Moreover, the Nb_2O_5/Al_2O_3 devices shows negligible *IV* temperature dependence (Fig. 3(b)) indicating the dominance of tunneling conduction, in agreement with findings in [1-3].

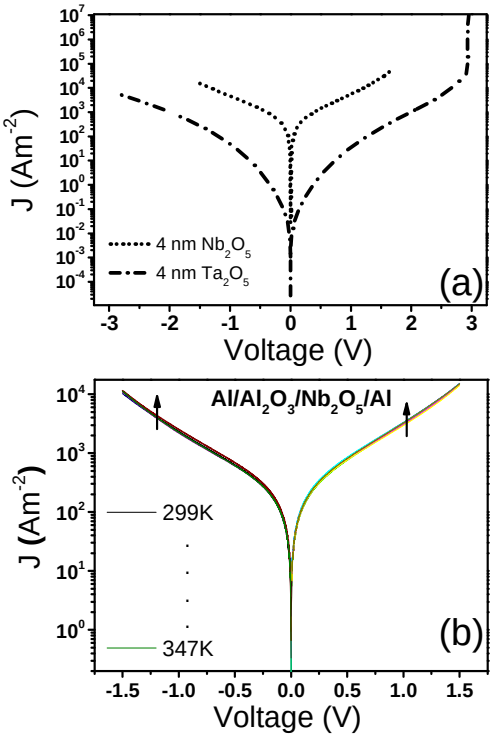

Fig.3: (a) JV plots of the Al/native oxide/1 nm Al_2O_3/I/Al MIIM devices, where I refers to Ta_2O_5 or Nb_2O_5. (b) Temperature dependent JV plots of the Nb_2O_5/Al_2O_3 MIIM device. The device area is: A = 10^{-8} m^2.

The large signal rectification is ascribed to the device asymmetry defined as the ratio of current at positive (I_+) or negative (I_-) bias, whichever larger, to that at opposite bias

$$\eta_{asym} = |I_+/I_-| \text{ or } |I_-/I_+| . \quad (1)$$

Small signal rectification, however, is governed by nonlinearity around the operating point and is usually realized by square law rectification. A measure of small signal nonlinearity is responsivity, defined as the ratio of dc rectified current, I_{dc} to input ac power, P_{in} [14].

$$Resp = \frac{I_{dc}}{P_{in}} = \frac{1}{2}\frac{I''}{I'}\bigg|_{V_p} = \frac{1}{2}\frac{dg_d/dV}{g_d} \quad (2)$$

where I' and I'' are the first and second derivatives of current and g_d is dynamic conductance at operating point V_p. Maraghechi *et al.* [3] have defined a nonlinearity factor as the ratio of dynamic to static conductance i.e.

$$\chi = \frac{dI/dV}{I/V} , \quad (3)$$

and also used the rate of change in nonlinearity, to reflect the small signal nonlinearity. The large signal asymmetry i.e. $|I/I_+|$ for Nb_2O_5/Al_2O_3 and Ta_2O_5/Al_2O_3 MIIM devices is shown in Fig. 4. The Ta_2O_5 device has peak value of 18 at around 0.3 V and at voltages close to 0 V. The Nb_2O_5/Al_2O_3 MIIM device shows the peak value of 7.6 around 0 V and the asymmetry reaches to ~ 6 at larger voltages.

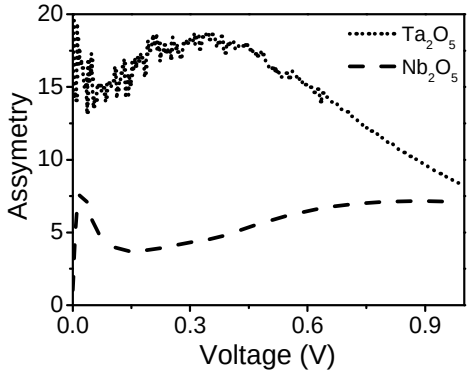

Fig.4: Device asymmetry (= $|I/I_+|$) for: 1 nm Al_2O_3/4 nm Ta_2O_5, and 1 nm Al_2O_3/4 nm Nb_2O_5 MIIM devices.

The responsivity vs voltage graphs for the MIIM devices are shown in Fig. 5, with peak values of 9 A/W and 6 A/W for Nb_2O_5 and Ta_2O_5 devices, respectively. The thickness of dielectric layers in these devices is 5.9 nm for Nb_2O_5, 5.3 nm for Ta_2O_5, and 1.6 nm for Al_2O_3, measured by VASE.

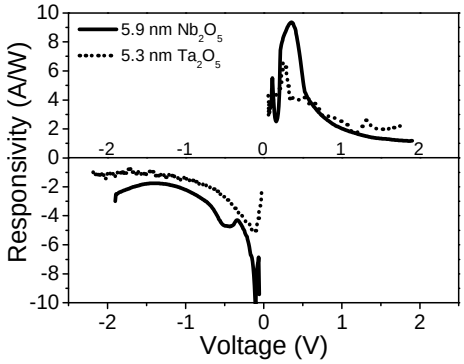

Fig.5: Device responsivity (= I″/2I′) for two MIIMs based on Al_2O_3/Ta_2O_5 & Al_2O_3/Nb_2O_5.

The nonlinearity factor for the above devices is shown in Fig. 6. The rate of change in nonlinearity factor at low voltage range <0.8 V was found to be 7.5 V^{-1} and 6.8 V^{-1} for Ta_2O_5 and Nb_2O_5 MIIM devices, respectively, higher than reported value of 5.5 V^{-1} [3].

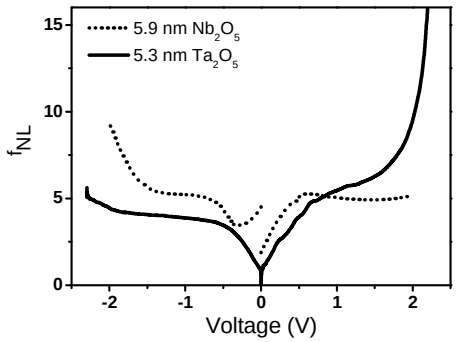

Fig.6: Device nonlinearity factor for two MIIMs based on Al_2O_3/Ta_2O_5 & Al_2O_3/Nb_2O_5.

3.3 Observation of resonant tunneling

A fingerprint of resonant tunneling can be found from a change of curvature and significant increase of current in *IV* characteristics. A larger current for positive bias is evident from Fig. 7a for Ta_2O_5/Al_2O_3 MIIM device. The native oxide grown unintentionally on bottom Al contact (~1.6 nm measured by VASE) has a large impact on the MIIM device behavior, particularly on resonant tunneling. It increases the thickness of Al_2O_3 layer, resulting in a shift of RT to larger voltages and in some cases beyond the operating voltages of the device. As can be seen from Fig. 7(b), after etching native Al_2O_3, the device shows a significant increase of current for about two orders of magnitude. The change in slope of the *JV* characteristics due to RT has moved from 2 V for the unetched sample to ~1.5 V for the etched sample.

Referring to the experimental data in Fig. 7 and theoretical calculations [11], the band diagrams shown in Fig. 8 can be derived. At small positive bias voltages (Fig. 8a), the conduction in both oxide layers is by direct tunneling (DT). By increasing the voltage, the conduction in the Ta_2O_5 layer is by Fowler-Nordheim (FN) and in Al_2O_3 by DT (Figs. 8b,d). However, the change in current at negative bias (Fig. 7(b)) is higher due to lowering of the barrier for Ta_2O_5, and at ~ -1.2 V the conduction changes to step tunneling (Fig. 8e). At larger positive voltages, > 1.5 V, when the bound states are established in the quantum well (Fig. 8c), the RT becomes dominant. A sharp increase in current and change of curvature can be observed at
~ 2 V in Fig. 7. Since the breakdown voltage for Ta_2O_5/Al_2O_3 MIIM devices is ~ 3 V (see Fig. 3(a)), the latter can be assigned to the onset of RT. It is worth mentioning that by calculations [11], the onset of resonant tunneling is expected to be at 1.5 V. The larger onset of around 2 V is presumably due to thicker alumina native oxide layer or a slight difference in work functions for the Al top and bottom contacts.

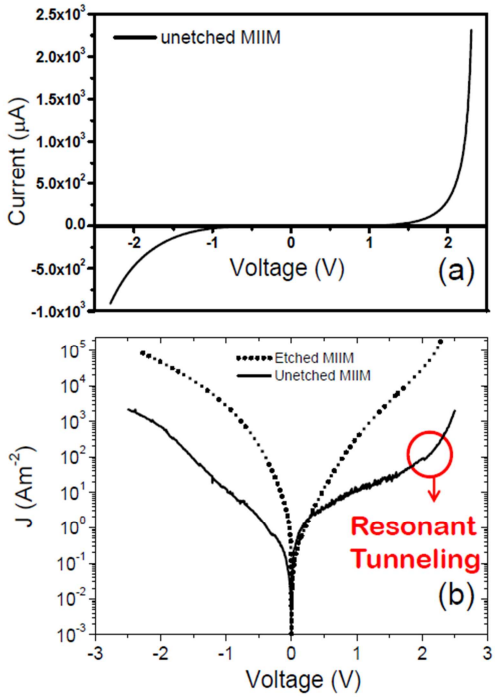

Fig.7: (a) IV (linear scale) and (b) J-V (log scale) plots with Al_2O_3/Ta_2O_5 MIIM prior and post etching of native Al_2O_3 on bottom Al electrode ($A = 10^{-8}$ m^2). The etching step and subsequent insulator deposition were done without breaking the vacuum. The onset of resonant tunnelling is marked.

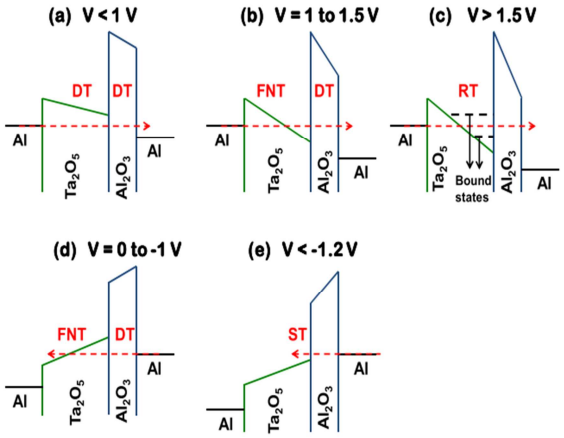

Fig.8: Energy band diagrams of Al/native oxide + 1 nm Al_2O_3/4 nm Ta_2O_5/Al MIIM tunnel rectifier depicting various conduction scenarios being dependent on external bias: (a)-(c) positive voltages; (d)-(e) negative voltages. DT, FN, ST, and RT refer to direct, Fowler-Nordheim, step and resonant tunneling, respectively.

4. Conclusions

We demonstrate experimentally, enhanced low voltage nonlinearity in ALD and rf sputtered nanometer scale bilayer Ta_2O_5/Al_2O_3 and Nb_2O_5/Al_2O_3 tunnel barriers. The results indicate how the layers can be designed to tune *IV* asymmetry and nonlinearity via resonant tunneling in these next-generation high speed rectifiers.

Acknowledgements. The work has been funded by EPSRC, UK, under project EP/K018930/1.

References

[1] N. Alimardani and J. Conley Jr., J. Appl. Phys. 105 (2014) 082902.
[2] N. Alimardani and J. F. Conley, Jr., Appl. Phys. Lett. 102 (2013) 143501.
[3] P. Maraghechi, A. Foroughi-Abari, K. Cadien, and A. Y. Elezzabi, Appl. Phys. Lett. 99 (2011) 253503.
[4] S. Grover and G. Moddel, Solid-State Electron. 67 (2012) 94.
[5] F. Aydinoglu, M. Alhazmi, B. Cui, O. M. Ramahi, M. Irannejad, A. Brzezinski, and M. Yavuz, J. N. Nanotechnol. 1 (2014) 3.
[6] P. Maraghechi, A. Foroughi-Abari, K. Cadien, and A. Y. Elezzabi, Appl. Phys. Lett. 100 (2012) 113503.
[7] M. N. Gadalla, M. Abdel-Rahman, and Atif Shamim, Scient. Rep. 4 (2014) 4270-1.
[8] S. Grover and G. Moddel, , IEEE J. Photov. 1 (2011) 78.
[9] S. Krishnan, E. Stefanakos and S. Bhansali, Thin Solid Films 516 (2008) 2244.
[10] N. Alimardani, E. W. Cowell, J. F. Wagner, J. F. Conley, D. R. Evans, M. Chin, S. J. Kilpatrick, and M. Dubey, J. Vac. Sci. Technol A. 30 (2012) 01A113.
[11] N. Sedghi, J. W. Zhang, J. F. Ralph, Y. Huang, I. Z. Mitrovic, and S. Hall, Proc. ESSDERC (2013, Romania) 131.
[12]H.G. Tompkins, E.A. Irene, *Handbook of Ellipsometry* (William Andrew, Norwich, NY, Springer), 2006.
[13] C. Wyon, Nuclear Instrumentation and Methods in Physical Res. B 186 (2002) 380.
[14] T. C. L.G. Sollner, W.D Goodhue, P. E. Tannenwald, C. D Parker and D. D. Peck, Appl. Phys. Lett. 43 (1983) 588.